Accelerated Adaptive Error Control and Refinement for SIE Scattering Problems

Jake J. Harmon, *Graduate Student Member, IEEE*, and Branislav M. Notaroš, *Fellow, IEEE*

Abstract—We present an application of adjoint-based adaptive error control and refinement for scattering problems solved using the method of moments (MoM) in the Electric Field Integral Equation (EFIE) and the coupled EFIE and Magnetic Field Integral Equation (MFIE) formulations. Specifically, we examine the Poggio-Miller-Chang-Harrington-Wu-Tsai (PMCHWT) formulation of the EFIE-MFIE. We first construct the adjoint problems of the EFIE and the EFIE-MFIE for estimating the error of radar cross-section (RCS) quantities of interest (QoIs) directly. We then introduce an effective adaptive refinement algorithm, based on an error prediction heuristic and *a posteriori* error estimation, which enables rapid and consistent convergence regardless of a chosen tolerance and the coarseness of the starting discretization. The approach, moreover, inherently promotes equilibration of the QoI error contributions and produces, therefore, consistently balanced meshes. Numerical examples with canonical scattering targets and adaptive p-refinement confirm the strength of the proposed refinement method, demonstrating the ability to generate high quality discretizations, both in terms of accuracy and efficiency, without expert user-intervention.

Index Terms—adaptive error control, adaptive mesh refinement, adjoint methods, computational electromagnetics, error estimation, higher order modeling, method of moments, radar cross-section, surface integral equations.

I. Introduction

IN the analysis of dielectric and metallic structures, whether for the design and simulation of antennas, aircraft, and other objects, the surface integral equation (SIE) approach provides a highly effective tool. By introducing electric and magnetic surface currents over the boundaries of homogeneous structures and discretizing the SIE problem by the method of moments (MoM), the unknown current densities may be found [1]–[3]. However, the choice of the approximation (e.g., the resolution of the surface or the number of degrees of freedom to model the currents) presents significant challenge in conducting accurate *and* efficient simulations for practical applications.

Electromagnetic modeling through the finite element method (FEM) has seen a significant research investment in error estimation and adaptive refinement to reduce the need for expert users in generating quality discretizations. Early approaches estimated the error of the solution or some property of the solution as an error indicator for refinement, see,

for example, [4]–[10]. Further approaches to adaptive FEM have explored goal-oriented error estimation and adaptive refinement [11]–[19].

Goal-oriented adaptivity, as opposed to standard residual or other less computationally expensive smoothness estimators and indicators (e.g., gradient jump methods), permits a significant enhancement of the refinement process [20]. Rather than address the accuracy of the solution as a whole, resources are allocated (or deallocated) to enhance the accuracy and efficiency of computing a quantity of interest (QoI). The use of adjoint-based methods facilitates the enhancement of numerical simulations for a variety of applications including goal-oriented error estimation through the dual-weighted residual (DWR) by delivering error *estimates* as opposed to just error *indicators* [20]–[22], though at the expense of solving an additional global problem. In addition to error estimation, in CEM, similar adjoint techniques have been applied to sensitivity analysis [23]–[26], and optimization [27], [28].

An efficient refinement procedure, while beneficial for FEM approaches, is of particular importance when applying the MoM for solving SIE problems. Each iteration, therefore, should refine (or coarsen) to the full extent of profitability, rather than some arbitrary fraction of the estimated discretization error as commonly performed. Moreover, in order to reduce the number of iterations required for highly accurate simulations (e.g., to reduce the number of matrix solves required), the adaptive procedure should dictate not only the *scope*, but also the *depth* of refinement, rather than fixed increments (or decrements) in resolution.

Aside from [29], [30], which focused specifically on geometrical-based refinement for scatterers with sharp edges, the limited existing literature on refinement (and error estimation in general) for SIE methods has largely focused on examining various residuals or some property of the solution as a surrogate for the quality of discretization, as in early approaches in FEM. For example, [31], proposed computing a residual through an overdetermined system for h-refinement in the EFIE problem. Similarly, a gradient jump error indicator and residual indicators obtained from an overdetermined system and from the boundary conditions on the tangential and normal electric fields were applied for the EFIE and p-refinement in [32]. Furthermore, a pair of discontinuity error indicators in the form of the jump of the charge and current at cell boundaries was introduced in [33] and applied in [34], [35] with comparison to a standard residual estimator for h-refinement in the EFIE problem. For the CFIE solved with the discontinuous Galerkin method, [36] applied a residual-based error estimator for non-conformal h-refinements when a cell exceeded an arbitrary threshold.

Jake J. Harmon and Branislav M. Notaroš are with the department of Electrical and Computer Engineering, Colorado State University, Fort Collins, CO 80523-1373 USA (e-mail: jake.harmon@ieee.org, branislav.notaros@colostate.edu).

Notably, in [37], goal-oriented error estimation using similar duality arguments as in this paper was leveraged for the computation of multi-port impedance parameters in the EFIE problem. In this manuscript, however, we study the EFIE and the Poggio-Miller-Chang-Harrington-Wu-Tsai (PM-CHWT) formulation ([38]–[40]) of the coupled EFIE-MFIE problem for accelerating the adaptive mesh refinement procedure to accurately compute the radar cross-section (RCS) of scattering targets. Moreover, we demonstrate that, through proper error estimation and refinement categorization, the dependence of the accuracy on the number of iterations may be heavily reduced. In particular, we extend the approach originally proposed in [19] for 3-D FEM to accelerate the refinement procedure for the SIE problem and metallic and composite scatterers. In contrast to existing approaches in SIE adaptivity, our approach attains an user desired accuracy rapidly and with a near-independence of the tolerance and number of iterations. Furthermore, our approach results in significantly improved mesh efficiency and error contribution equilibration through intelligent automatic resource allocation driven by a combination of an *a priori* error behavior heuristic and *a posteriori* error estimation.

The rest of the paper is organized as follows. Section II outlines the adjoint problem of the PMCHWT formulation of the coupled EFIE-MFIE, starting with the EFIE, and introduces a customizable scattering QoI as well as an RCS QoI to drive the adaptivity procedure. Section III describes the DWR expression of the error, where the solution of the global adjoint problem in an enriched space coupled with a combined *a priori-a posteriori* heuristic permits accelerating the refinement procedure through error prediction. Section IV includes numerical examples, indicating the ability of the proposed refinement procedure to produce highly accurate discretizations rapidly. The examples illustrate the inherent acceleration of refinement provided by the approach. Finally, the results indicate that the method successfully improves mesh equilibration, indicating the efficiency of the resultant discretizations.

II. THE ADJOINT EFIE AND EFIE-MFIE (PMCHWT) PROBLEMS

A. Problem Formulations

We first outline the general procedure for deriving the dual (or adjoint) problem for a given forward problem,

$$\mathcal{L}\mathbf{u} = \mathbf{f} \qquad (1)$$

involving the forward solution $\mathbf{u}$ and an excitation $\mathbf{f}$, which is described either by a differential or integral equation, with an associated variational formulation: Find $\mathbf{u} \in B$ such that

$$a(\mathbf{u}, \, \boldsymbol{\phi}) = \langle \mathbf{f}, \, \boldsymbol{\phi} \rangle \quad \forall \boldsymbol{\phi} \in B, \qquad (2)$$

where B denotes the trial and test space, $\langle \cdot, \cdot \rangle$ denotes the standard L^2 inner-product (linear in the first argument and antilinear in the second), and a denotes the sesquilinear form generated by $\mathcal{L}$.

From the Lagrange identity [21],

$$\langle \mathcal{L}\mathbf{u}, \mathbf{v} \rangle = \langle \mathbf{u}, \mathcal{L}^*\mathbf{v} \rangle, \qquad (3)$$

we find the defining equality for constructing the adjoint operator $\mathcal{L}^*$ associated with the adjoint problem

$$\mathcal{L}^*\mathbf{v} = \mathbf{p} \qquad (4)$$

for an excitation $\mathbf{p}$, along with its own variational formulation involving the adjoint sesquilinear form a^*, analogous to that of (2).

Starting from the left-hand-side of the Lagrange identity, we manipulate the inner-product, mainly through integration by parts, to transform the operations on the forward solution $\mathbf{u}$ onto the adjoint solution $\mathbf{v}$. In the process of performing these operations, the requirements of $\mathbf{v}$, which we assume at first to be an arbitrary function, unfold, namely the differentiability, integrability (including in the sense of the Cauchy principal value, as is necessary in the case of the EFIE and the coupled EFIE-MFIE), etc., and the boundary conditions. These operations typically result in terms on the boundary (e.g., line integrals) which, in total, must be equal to zero [21].

Let us first study the EFIE separately, assuming PEC structures.

We have the boundary condition on the electric field

$$[\mathbf{E}(\mathbf{J}_S, \varepsilon_1, \mu_1)]_{\text{tang}} + (\mathbf{E}_i)_{\text{tang}} = 0, \qquad (5)$$

for complex permittivity ε_1 and complex permeability μ_1.

The scattered field in the region of complex permittivity ε and complex permeability μ is

$$\mathbf{E} = \mathbf{E}_J(\mathbf{J}_S) = \mathcal{L}_{\text{EE}}\mathbf{J}_S, \qquad (6)$$

where

$$\mathcal{L}_{\text{EE}}\mathbf{J}_S = -j\omega\mathbf{A} - \nabla V,$$
$$\mathbf{A} = \mu \int_{S'} \mathbf{J}_S g \, dS', \quad V = \frac{j}{\omega\varepsilon} \int_{S'} \nabla'_S \cdot \mathbf{J}_S g \, dS',$$
$$g = \frac{e^{-\gamma R}}{4\pi R} = \frac{e^{-\gamma|\mathbf{r}-\mathbf{r}'|}}{4\pi|\mathbf{r} - \mathbf{r}'|} \qquad (7)$$

where ω denotes the angular frequency and γ denotes the complex-valued propagation coefficient in the medium [1]–[3]. Furthermore, in line with (2), we let a_{EE} denote the sesquilinear form generated by $\mathcal{L}_{\text{EE}}$ with $B \subset H(\text{div}; \Omega)$, where Ω denotes a 2-D manifold embedded in 3-D space, as derived in [1]. A detailed description of the EFIE, as well as the PMCHWT formulation of the EFIE-MFIE may be found in [2], along with comparisons to the other formulations of the SIE problem (e.g., the combined field integral equation).

Starting from the Lagrange identity (3) and with the adjoint solution $\mathbf{v}_E$, the goal is to identify the adjoint operator $\mathcal{L}_{\text{EE}}^*$ such that

$$\langle \mathcal{L}_{\text{EE}}\mathbf{J}_S, \mathbf{v}_E \rangle = \langle \mathbf{J}_S, \mathcal{L}_{\text{EE}}^*\mathbf{v}_E \rangle, \qquad (8)$$

Peforming integration by parts on the left-hand side of (8) and taking that $\mathbf{v}_E \in B \subset H(\text{div}; \Omega)$, as for the forward solution, satisfies each condition (such as the required integrability), and due to the normal continuity, the resulting line boundary terms vanish. In other words, the line boundary terms vanish in the same way as for the weak form of the forward problem, e.g., as in [1]–[3].

Hence, we have the final form for the adjoint operator,

$$\mathcal{L}_{\text{EE}}^* \mathbf{v}_E = j\omega\mu^* \int_S \mathbf{v}_E g^* \, dS + \frac{j}{\omega\varepsilon^*} \int_S \nabla'(g^* \nabla_S \cdot \mathbf{v}_E) \, dS, \quad (9)$$

of the EFIE problem.

Most importantly, however, for finding the Galerkin approximate solution (i.e., when B is finite dimensional), the formation of the Galerkin system matrix for the adjoint problem amounts to exchanging the roles of the trial and test functions (i.e., taking the transpose) and, due to the definition of the inner-product, taking the complex conjugate relative to the Galerkin system matrix of the associated forward problem.

That is, rather than considering an adjoint variational formulation of (6) explicitly, we need only find $\mathbf{v}_E \in B$ such that

$$a_{\text{EE}}(\phi, \mathbf{v}_E) = \langle \phi, \mathbf{p} \rangle \quad \forall \phi \in B, \quad (10)$$

where the ordering of the trial function $\mathbf{v}_E$ and test function ϕ in relation to the pattern of the sesquilinear form for the forward problem (2) is of critical importance. Note, however, that as the EFIE is symmetric, the solution of the adjoint problem is simplified as in the case of the forward problem, which provides an efficiency enhancement to the analysis of PEC targets.

Now that we formed the adjoint problem associated with the EFIE (for PEC materials), let us consider the procedure applied to the coupled EFIE-MFIE problem for composite structures.

In the EFIE-MFIE case, we have the following set of boundary conditions:

$$[\mathbf{E}(\mathbf{J}_S, \mathbf{M}_S, \varepsilon_1, \mu_1)]_{\text{tang}} + (\mathbf{E}_i)_{\text{tang}} = [\mathbf{E}(-\mathbf{J}_S, -\mathbf{M}_S, \varepsilon_2, \mu_2)]_{\text{tang}}, \quad (11)$$

$$[\mathbf{H}(\mathbf{J}_S, \mathbf{M}_S, \varepsilon_1, \mu_1)]_{\text{tang}} + (\mathbf{H}_i)_{\text{tang}} = [\mathbf{H}(-\mathbf{J}_S, -\mathbf{M}_S, \varepsilon_2, \mu_2)]_{\text{tang}}, \quad (12)$$

with $\varepsilon_1, \mu_1, \varepsilon_2, \mu_2$ representing the complex valued material parameters outside and inside the scatterer, respectively. Considering the PMCHWT formulation of the EFIE-MFIE exclusively, the scattered field in the region of complex permittivity ε and complex permeability μ is

$$\mathbf{E} = \mathbf{E}_J(\mathbf{J}_S) + \mathbf{E}_M(\mathbf{M}_S) = \mathcal{L}_{\text{EE}}\mathbf{J}_S + \mathcal{L}_{\text{EM}}\mathbf{M}_S, \quad (13)$$

and, likewise, the scattered magnetic field in the region of complex permittivity ε and complex permeability μ is

$$\mathbf{H} = \mathbf{H}_M(\mathbf{M}_S) + \mathbf{H}_J(\mathbf{J}_S) = \mathcal{L}_{\text{MM}}\mathbf{M}_S + \mathcal{L}_{\text{ME}}\mathbf{J}_S, \quad (14)$$

where

$$\mathcal{L}_{\text{EM}}\mathbf{M}_S = -\frac{1}{\varepsilon}\nabla \times \mathbf{F},$$

$$\mathbf{F} = \varepsilon \int_{S'} \mathbf{M}_S g \, dS', \quad \mathcal{L}_{\text{MM}}\mathbf{M}_S = -j\omega\mathbf{F} - \nabla U, \quad (15)$$

$$\mathcal{L}_{\text{ME}}\mathbf{J}_S = \frac{1}{\mu}\nabla \times \mathbf{A}, \quad U = \frac{j}{\omega\mu}\int_{S'}\nabla_S' \cdot \mathbf{M}_S g \, dS',$$

and with $\mathbf{E}_J$ as in the EFIE expression, see [1]. For this coupled problem, we then have the variational formulation: Find $\mathbf{u} = \{\mathbf{J}_S, \mathbf{M}_S\} \in B \subset H(\text{div}; \Omega) \times H(\text{div}; \Omega)$ such that

$$a_{\text{E-M}}(\mathbf{u}, \phi) = \langle \mathbf{f}, \phi \rangle \quad \forall \phi \in B, \quad (16)$$

where $a_{\text{E-M}}$ represents the sesquilinear form generated by (13) and (14) [1], and $\mathbf{f}$ is the excitation formed by the incident electric and magnetic fields as in (11) and (12).

The form of the adjoint problem may be found by first considering a single region (e.g., the exterior region) separately in (13) and (14) due to the operational symmetry. Furthermore, in the same manner as for the EFIE, from the Lagrange identity (3), constructing the Galerkin system matrix for the dual EFIE-MFIE mechanically only requires exchanging the roles of the trial and test functions (i.e., the transpose of the system matrix) and taking the complex-conjugate (due to the definition of inner-product) of the Galerkin system matrix of the associated forward problem. Explicitly, for the adjoint solution of the coupled EFIE-MFIE, we seek $\mathbf{v} = \{\mathbf{v}_E, \mathbf{v}_M\} \in B$ such that

$$a_{\text{E-M}}(\phi, \mathbf{v}) = \langle \phi, \mathbf{p} \rangle \quad \forall \phi \in B, \quad (17)$$

(once again noting the position of the trial and test functions) where, in this case, as both the electric and magnetic current densities in the forward belong to $H(\text{div}; \Omega)$ as noted above, $B \subset H(\text{div}; \Omega) \times H(\text{div}; \Omega)$.

B. Computing the Excitation for the Adjoint Problem

To build an excitation for the specified adjoint problems, as in [19], we consider a linear functional J of the forward solution $\mathbf{u}$, where, according to Riesz representation theorem, there exists $\mathbf{p}$, known as the Riesz representation of J, such that for all $\mathbf{u}$

$$J[\mathbf{u}] = \langle \mathbf{u}, \mathbf{p} \rangle, \quad (18)$$

and where $\mathbf{p}$ represents the same quantity in the definition of the adjoint problem (4). We note that solving the dual problem, either for the dual EFIE or the coupled dual EFIE-MFIE, does not require an explicit form for $\mathbf{p}$ as only the ability to evaluate the QoI itself is necessary; i.e., as depicted in (17), we need only compute

$$\langle \phi, \mathbf{p} \rangle = J[\phi], \quad (19)$$

for all the test functions ϕ.

In the following examples, we study the radar cross-section (RCS) of the scattering target. While scalar, the RCS is not inherently a linear functional of the scattered field $E^{sc}[\mathbf{u}]$,

$$\mathbf{E}^{sc}[\mathbf{u}] = \left(-j\omega\mu \int_S \mathbf{J}_S g + k^{-2}\nabla_S \cdot \mathbf{J}_s \nabla g \, dS + \int_S \mathbf{M}_S \times \nabla g \, dS\right), \quad (20)$$

which *is* a linear functional of $\mathbf{u}$, and therefore must first be linearized. Examining the RCS, which we denote by σ, we have that

$$\sigma = \lim_{r \to \infty}\left(4\pi r^2 \frac{|\mathbf{E}^{sc}|^2}{|\mathbf{E}^{inc}|^2}\right), \quad (21)$$

where, for simplicity, instead of treating (21) in the limit, let us assume that r is fixed sufficiently far away (i.e., $r >> \lambda$, where λ denotes the wavelength). Note, of course, that the RCS in (21) implicitly depends on the scattering angle. Naturally, the scattered field (20) may be employed as a proxy for the RCS, albeit with a detriment to the efficiency of the

refinement for the overall objective as only the magnitude of the scattered field is relevant (as opposed to the full complex valued quantity) and, since the right-hand side of the adjoint problem demands a scalar QoI, one adjoint excitation would be required for each component of the scattered electric field for full reconstruction.

Now, as $|\mathbf{E}^{sc}|^2 = (\mathbf{E}^{sc})^{\mathrm{H}}\mathbf{E}^{sc}$ is not analytic, the linearization of the RCS must be performed by considering the Wirtinger derivatives. Hence, we have that the first order expansion of the RCS about a reference point $\mathbf{E}_0$ is

$$\sigma(\mathbf{E}^{sc}) \approx \sigma(\mathbf{E}_0) + 2\mathrm{Re}\left\{\frac{\partial\sigma}{\partial\mathbf{E}^{sc}}(\mathbf{E}^{sc} - \mathbf{E}_0)\right\}, \qquad (22)$$

where

$$\frac{\partial\sigma}{\partial\mathbf{E}^{sc}} = \frac{1}{2}\left(\frac{\partial\sigma}{\partial\mathrm{Re}(\mathbf{E}^{sc})} - j\frac{\partial\sigma}{\partial\mathrm{Im}(\mathbf{E}^{sc})}\right) \qquad (23)$$

denotes the first Wirtinger derivative.

Expanding (22) by the evaluation of (23), we have that

$$\sigma(\mathbf{E}^{sc}) \approx \sigma(\mathbf{E}_0) + 8\pi r^2 \mathrm{Re}\left\{\mathbf{E}_0^{\mathrm{H}}(\mathbf{E}^{sc} - \mathbf{E}_0)\right\}, \qquad (24)$$

which completes the first order approximation of the RCS.

Now, as for the application of this quantity to form the excitation of the adjoint problem, two additional changes must be made. Firstly, taking the real part is not a linear operation in $\mathbb{C}$ and therefore violates the requirements of the QoI. Secondly, (24) is otherwise an affine function. These two obstacles motivate the construction of the following QoI, which satisfies the requirements for the DWR error estimation,

$$J[\mathbf{u}; \mathbf{E}_0] = 8\pi r^2 \mathbf{E}_0^{H}\mathbf{E}^{sc}[\mathbf{u}], \qquad (25)$$

where, as noted above, $r \gg \lambda$.

To evaluate the effectiveness of this QoI for estimating the error of the RCS, let us take two approximations of the solution $\mathbf{u}$, $\mathbf{u}_1$ and $\mathbf{u}_2$, and the corresponding approximations of the scattered field $\mathbf{E}_1^{sc}$ and $\mathbf{E}_2^{sc}$ for $r \gg \lambda$. From (24), we have that

$$\sigma(\mathbf{E}_1^{sc}) - \sigma(\mathbf{E}_2^{sc}) \approx 8\pi r^2 \mathrm{Re}\left\{\mathbf{E}_0^{H}(\mathbf{E}_1^{sc} - \mathbf{E}_2^{sc})\right\}, \qquad (26)$$

which, from (25), is equivalent to $\mathrm{Re}\{J[\mathbf{u}_1 - \mathbf{u}_2; \mathbf{E}_0]\}$. In other words, computing the error for the QoI (25) produces the same error (after extracting just the real component) as for the first order expansion (24).

As for the reference point $\mathbf{E}_0$, we note that the adjoint problem, when solved after the forward problem, has access to the approximate solution to the forward problem (and therefore its own estimate of the RCS and the scattered field). Hence, $\mathbf{E}_0$ is taken as this estimate of the scattered field. As the adaption method (described in Section III) proceeds iteration by iteration and the quality of the discretization improves, $\mathbf{E}_0$ is similarly enhanced, resulting in improved agreement between the linearized RCS (24) and the actual RCS. Moreover, as a consequence of this improved agreement, the quality of (25) for estimating the error in RCS for refinement increases.

Finally, just as in the forward problem, where multiple excitations may be solved for limited cost (when using a direct solver), multiple QoIs (e.g., multiple scattering angles) may be solved for efficiently through simple substitution of multiple right-hand sides. Of course, in the adaptive refinement process handling multiple QoIs in this manner requires accumulating the refinement directives such that a single discretization yields the desired accuracy for the entire QoI collection.

III. ERROR ESTIMATION AND ADAPTION

With the adjoint solution computed (either for a single QoI or multiple), the estimation of the QoI error contributions proceeds in an identical fashion to [19]. The error induced by solving the integro-differential equation approximately,

$$\mathbf{e} = \mathbf{u} - \mathbf{u}_p, \qquad (27)$$

where $\mathbf{u}_p \in B_p$ represents the Galerkin approximate solution for a finite dimensional subspace $B_p \subset H(\mathrm{div};\Omega)$ (for the EFIE) or $B_p \subset H(\mathrm{div};\Omega) \times H(\mathrm{div};\Omega)$ (for the coupled EFIE-MFIE), translates to an error in the functional

$$J[\mathbf{e}] = J[\mathbf{u}] - J[\mathbf{u}_p] \qquad (28)$$

by linearity of J. From (18) and the Lagrange identity (3), this error may be further expressed as

$$\begin{aligned} J[\mathbf{e}] &= \langle\mathbf{e}, \mathbf{p}\rangle \\ &= \langle\mathcal{L}\mathbf{e}, \mathbf{v} - \boldsymbol{\psi}_p\rangle \\ &= \langle\mathbf{f}, \mathbf{v} - \boldsymbol{\psi}_p\rangle - a(\mathbf{u}_p, \mathbf{v} - \boldsymbol{\psi}_p), \end{aligned} \qquad (29)$$

for arbitrary $\boldsymbol{\psi}_p \in B_p$ (due to Galerkin orthogonality) and where a denotes the sesquilinear form, either for the EFIE or the EFIE-MFIE, with $\mathbf{v}$ representing the respective solution to the adjoint problems defined in (10) or (17) for the choice of the QoI. While the choice of $\boldsymbol{\psi}_p$ does not affect the evaluation of $J[\mathbf{e}]$, the choice of $\boldsymbol{\psi}_p = \boldsymbol{\Pi}_p\mathbf{v}$, the projection of the adjoint solution $\mathbf{v} \in B$ onto the solution space of the forward problem B_p, tunes the resulting cellwise error contribution estimates by eliminating irrelevant contributions for the purposes of addressing the insufficient and inefficient regions of the discretization. If only an error estimate is required rather than adaptive refinement indicators, $\boldsymbol{\psi}_p = 0$ may be chosen to eliminate the subtraction in (29). The evaluation of (29) quantifies the contributions of the approximation error of the electric current densities and magnetic current densities (for the coupled EFIE-MFIE) to the error in the functional J, with the computations required (i.e., for evaluating the inner-product and sesquilinear form in (29)) of the same manner as required for the filling of the Galerkin system matrix.

The previous expressions assume access to the exact adjoint solution $\mathbf{v}$; however, in general we must substitute a numerical approximation. To produce a usable (i.e., non-zero) estimate, we opt to solve the adjoint problem for $\mathbf{v}_{p_+} \in B_{p_+}$, where $B_{p_+} \supset B_p$ denotes the enriched space produced by increasing the expansion orders of every cell in the discretization of the forward problem by one, as seeking the approximate solution to the adjoint problem in the same space as the forward solution results in an estimate of zero error due to Galerkin orthogonality. While increasing the polynomial order provides excellent error estimation information, cheaper alternatives, such as those discussed in [20], may be more suitable for certain applications. Additionally, with regards to the approximation of the adjoint solution, similarly to

the demonstrations in [41], the QoI error estimate depends simultaneously on the approximation error of the adjoint solution and the approximation error of the forward solution.

Of course, in contrast to the FEM case with contributions automatically localized to an individual cell, the proper accumulation of contributions in the case of the SIE problem is potentially ambiguous given the global interactions resulting from the Green's function. However, note that the assembly of (29) divides in a piecewise fashion according to interactions between pairs of cells and—within each pair of cells—a shape function for the forward solution and a shape function for the adjoint solution. Explicitly, for the error contribution estimate $\tilde{e}_i$ of cell i, $i = 1, \ldots, K$, we compute

$$\tilde{e}_i = \langle \mathbf{f}, \mathbf{v}_{p_+} - \mathbf{\Pi}_p \mathbf{v}_{p_+} \rangle_i - a_i(\mathbf{u}_p, \mathbf{v}_{p_+} - \mathbf{\Pi}_p \mathbf{v}_{p_+}), \qquad (30)$$

where the subscript i denotes the restriction of the inner-products over cell i, where, crucially, the portion of the adjoint solution under consideration is associated. Note that internally, the evaluation of the sesquilinear form in the error estimate traverses every cell in the discretization for the integration of the components related to the forward problem and its solution.

However, we note an exception to the contribution accumulation rule established in (30): when a contribution from a boundary DoF in the discretization of the adjoint problem (i.e., the normal component is non-zero on an edge for that DoF) arises due to the insufficient expansion order of a neighboring cell, the contribution is assigned entirely to that lower order neighbor to ensure that when treated as refinement indicators, the error contributions correctly identify the regions of the discretization that require improvement. Even so, this approach preserves the expression of the total QoI error so that

$$J[\mathbf{e}] \approx \sum_{i=1}^{K} \tilde{e}_i. \qquad (31)$$

The contributions, additionally, when accumulated per direction within each cell or individually for the electric and magnetic current densities, permits additional refinement classification information.

With adequate error estimates and refinement indicators, any successful adaptive error control strategy must drive two simultaneous developments in the discretization. Naturally, the primary goal of mesh adaption is to reach a termination condition in the overall error. However, the adaption must also encourage error homogenization. As shown in [42], the ideal discretization (i.e., the discretization which achieves both accuracy and efficiency) requires homogenization of error contribution estimates. Regions of a discretization with excessively large error contribution estimates, for example, indicate mesh insufficiency, while regions with null error contribution estimates indicates inefficiency and the profitability of coarsening.

In response to these complementary goals and to guide the adaptive refinement process, similarly to [19], we impose the following *a priori* local (i.e., interpolatory) p-refinement error convergence heuristic based on the theoretical solution error bounds derived in [43], which, while not strictly satisfied, facilitates both the determination of effective refinement

gradation to reduce the number of iterations required in the refinement procedure (i.e., to reduce the number of linear systems that must be solved to reach a desired accuracy) and the improvement of mesh equilibration:

$$|\tilde{e}_i| \approx C p_i^{-(r+1/2)}, \qquad (32)$$

where p_i denotes the degree of the polynomial basis on the cell, r denotes the Sobolev regularity of the solution, C is an unknown coefficient, and $\tilde{e}_i$ represents the known error contribution estimate computed in (30). While we exclusively study p-refinement in this manner, the same process may be repeated for guiding h-refinements. Note that this condition is based on derivations for the approximation error from [43], rather than the error in some functional or the contributions to the error in the functional as we are studying here. However, only a rough form relating the behavior of the local contributions to the error and discretization choices (namely, the size of the cell or its expansion order) is sufficient for acceleration, given the necessarily iterative refinement procedure.

By predicting refinements from the error contribution estimates computed in (30) via a suitable adjoint solution combined with the imposed convergence condition (32), we can map the existing properties of the discretization (e.g., the expansion orders and error contribution estimates on each cell) to update parameters that target the aforementioned adaptive refinement goals, namely to reach a desired accuracy with an awareness and promotion of equilibration.

As to the termination of the refinement procedure, we require that the absolute value of the error contribution estimate $\tilde{e}_i$ for each cell i falls below an absolute threshold T_{local} such that

$$|\tilde{e}_i| \leq T_{\text{local}}. \qquad (33)$$

Then, for an update equation of the expansion order on cell i, according to the termination condition (33), we would like to find $p' > p$ (in the case of refinement when $|\tilde{e}_i| > T_{\text{local}}$) such that

$$|\tilde{e}_i'| \approx C (p_i')^{-(r+1/2)} \approx T_{\text{local}}, \qquad (34)$$

where $\tilde{e}_i'$ denotes the predicted error contribution after increasing p to p'.

Now, while estimating the Sobolev regularity is possible (e.g., as in [44]), let us instead follow an alternative condition, namely that if we were to conduct p-refinement, then we should assume the solution is sufficiently regular such that p-refinement is profitable (otherwise, an h-refinement should be executed to "isolate" non-smooth behavior [45], [46]). In other words, for an as-of-yet unknown expansion order p', we assume that $r \geq p'$, and, in particular, for the purposes of leveraging (32) for an easily computable update equation, we take $r = p' + 1$.

Then, using the *a posteriori* error estimate to approximate C (i.e., $C \approx |\tilde{e}_i| p_i^{(r+1/2)}$), the predicted value of p' may be found by solving

$$\frac{p^{(p'+3/2)}}{p'^{(p'+3/2)}} - \frac{T_{\text{local}}}{|e_i|} = 0, \qquad (35)$$

for p' by, e.g., Newton's method. Furthermore, since an integer is needed, the ceiling of the value obtained from (35) is taken.

For coarsening when $|\tilde{e}_i| << T_{\text{local}}$, a similar approach can taken be taken. In this case, from (34) we seek $p' < p$ such that

$$p' = \left\lceil p \left(\frac{T_{\text{local}}}{|e_i|} \right)^{-1/(p+3/2)} \right\rceil, \qquad (36)$$

where the same regularity assumption as before was applied with the known value p as opposed to p'.

Note that especially in the case of h-refinements, the execution of the adaptivity directives is constrained by practical limitations, e.g., how a cell may be subdivided or combined with its neighbors (in the case of coarsening).

Of course, in practice we must also consider that a discretization may start in the preasymptotic region, in which case the degree of refinement in a single iteration should be truncated. Moreover, in such cases, the estimate of the absolute error might increase (temporarily) as the discretization improves. For pure p-refinement, the limiting case is simply increasing (or decreasing) the expansion order by 1, but often increases by 2 or 3 may be made with confidence. For automatic control of this limit, restrictions may be imposed on the max increase if the estimated relative error in the QoI,

$$\frac{|\sum_{i=1}^{K} \tilde{e}_i|}{|J[\mathbf{u}_p] + \sum_{i=1}^{K} \tilde{e}_i|}, \qquad (37)$$

exceeds some threshold. Furthermore, the coarsening facilitated by (36) permits correcting mistaken over-refinement.

We emphasize that the tolerance T_{local} is not a normalized quantity. Nevertheless, an automatic selection of T_{local} from a desired relative tolerance can be achieved even without prior knowledge of the magnitude of the QoI. From the initial discretization, a coarse computation of the QoI, while inaccurate, typically yields a result within an order of magnitude of the actual QoI, from which the necessary value for T_{local} may be found for a given desired overall relative error. As the discretization quality increases as well, updating the tolerance T_{local} each iteration based on the enhanced QoI data enables improved selection of the refinement criterion. In the numerical results section, from a desired relative global tolerance T_{rel}, we estimate the necessary local absolute tolerance T_{local} by selecting

$$T_{\text{local}} = \alpha \frac{T_{\text{rel}} \left| J[\mathbf{u}_p] + \sum_{i=1}^{K} \tilde{e}_i \right|}{K} \qquad (38)$$

where, since the tolerances cannot be satisfied exactly and given the effects of error cancellation, $\alpha > 1$ to provide a closer estimate of the necessary tolerance. In the numerical results section, we take $\alpha = 20$ as a reasonable amplification, which results in relative errors typically within an order of magnitude of the desired without further adaptivity. While the refinement procedure is not extremely sensitive to this choice, precise satisfaction of the desired relative error may require additional adaptivity.

Finally, we reiterate that given the practical limitations of how cells may be refined, i.e., how a cell is subdivided or that the expansion order must be a strictly positive integer, as well as the necessarily iterative nature of any refinement procedure, more sophisticated marking for acceleration is typically not necessary. The computed error contribution estimates may also be applied in more traditional ways, though perhaps with reduced mesh equilibration tendencies, such as with Dörfler marking [47], the dominant approach to marking cells for refinement, or hybridized with such approaches.

IV. NUMERICAL RESULTS

We now present a series of numerical examples that deploy the proposed SIE adaptive mesh refinement (AMR) technique for p-refinement. A similar procedure may applied in the case of h-refinement; however, effective h-refinement—particularly when working with quadrilateral patches as in this work—in practice relies heavily on proper remeshing or the handling of non-conformal cells, e.g., 1-irregular meshes, both of which are beyond the scope of this manuscript. In each case we start with an extremely coarse discretization (in terms of the accuracy) and we truncate the maximum increase of a given cell's expansions order in a single iteration by three, and, as a second restriction, we limit the maximum increase to one if the estimated global QoI relative error exceeds 10 (1000% error) to penalize the most significant over-refinements.

Finally, we emphasize that the computation of the error estimates as presented relies on solving the adjoint problem for the p-enriched space (by increasing the expansion orders by one relative to the discretization of the forward problem). The increase in the number of DoFs required for solving the higher-order adjoint problem is dependent on the size of problem and may therefore be substantial. As a mitigating factor in the expense of this approach, the computations for assembling the Galerkin system matrix for the adjoint problem may be reused for the forward problem (i.e., by extracting a subset of the system matrix) by employing hierarchical basis functions. Furthermore, the most expensive computations may be reused between iterations such that a small change in the discretization requires a small increase in computation time associated with the new entries in Galerkin system matrix that must be filled, in addition to solving the linear systems. In order to examine the quality of the discretizations produced according to this approach specifically, rather than the quality of the adjoint solution, in the following examples we report the QoI without the enhancement provided by the sum of the error contribution estimates that are otherwise employed to dictate refinements as described in Section III; i.e., where applicable, we depict $J[\mathbf{u}_p]$ as opposed to $J[\mathbf{u}_p] + \sum_{i=1}^{K} \tilde{e}_i$. A future work will explore enhancing the efficiency of the error estimation for SIE problems.

For the first example, we investigate application to a spherical scatterer for adaptive error control of the monostatic RCS. As outlined in Section II, we first compute the error contribution estimates according to the complex-valued QoI (25) and then discard the imaginary component to produce the error estimate for the real-valued linearized RCS (24) and the associated refinement indicators. We refine the scattering target to achieve an estimated relative QoI error of approximately $T_{\text{rel}} \in \{1 \times 10^{-1}, 1 \times 10^{-2}, 4 \times 10^{-3}, 1 \times 10^{-3}\}$ by computing appropriate absolute local tolerances as provided by (38). The desired relative QoI error is used only to compute

This article has been accepted for publication in IEEE Transactions on Antennas and Propagation. This is the author's version which has not been fully edited and content may change prior to final publication. Citation information: DOI 10.1109/TAP.2022.3177424

7

appropriate absolute local tolerances (updating each iteration); the termination of the refinement is provided exclusively by satisfaction of the local tolerances.

The first sphere has a complex relative permittivity of $\varepsilon_r = 2.56 - j0.05$, and the diameter is $3\lambda_0$ (where λ_0 denotes the wavelength in vacuum), which is analyzed with the coupled EFIE-MFIE in the PMCHWT formulation. We refer to this first scatterer by $S1$. The starting discretization, which consists of 216 geometrically bicubic elements with first order basis functions, is shown in Fig. 1. Geometrically, the relative error of the surface area compared to a perfect sphere is 1×10^{-5}. In terms of the accuracy of the solution, the discretization is very coarse as the percent error (with respect to the analytical value computed from Mie scattering) of the RCS computed from the starting discretization is 97% for $S1$. Note that unless otherwise specified, the RCS is not expressed in decibels to facilitate direct comparison of the actual relative error with the estimated relative error produced internally by the adaptive refinement procedure as in (37). Finally, in the illustrations of the following results, we normalize the error contribution estimates at each iteration by the estimated magnitude of the QoI at that iteration to produce relative local error contribution estimates. Conveniently, for the procedure applied to $S1$ as described above, this permits illustrating unified local (i.e., per-cell) relative tolerance refinement termination thresholds T_{S1Li} from (38) such that

$$T_{S1Lj} = \alpha \frac{T_{\text{rel}j}}{216}, \tag{39}$$

with j indexing the set of four relative tolerances above, as the absolute tolerances vary each iteration according to (38).
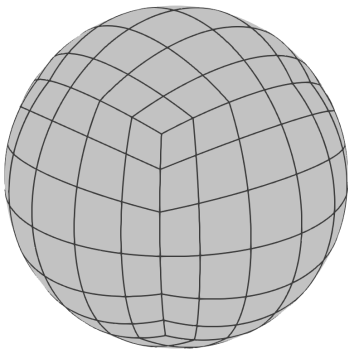

Fig. 1. The starting discretization for the spherical scatterer $S1$ with 216 geometrically bicubic elements.

We now conduct the AMR procedure as outlined in Section III. As shown in Fig. 2(a), all examples attain the desired relative local tolerances rapidly. Except for the second coarsest tolerance, which required four iterations, the refinement procedure attained the desired local error contribution tolerance in three iterations. Furthermore, as seen in Fig. 2(b), for each example, only the first iteration drives a large change in the discretization, introducing many new DoFs, while the remaining iterations tune the allocation of unknowns with small adjustments. As a result, storing (and reusing) the Galerkin integrals between iterations results in vast reductions in computation time.
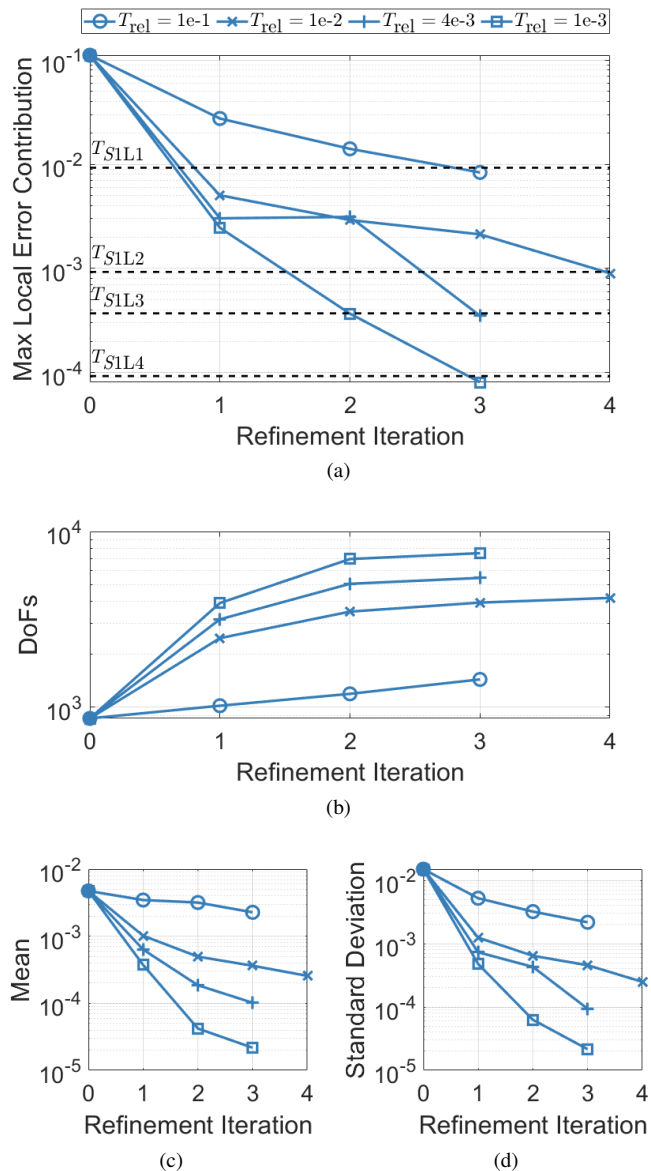

Fig. 2. Performance of the AMR algorithm for the spherical scatterer $S1$ for four tolerances. (a) Convergence of the relative maximum error contribution estimate versus the number of refinement iterations. (b) DoFs allocated by the AMR procedure at each iteration. (c) Mean of the relative error contribution estimates. (d) Standard deviation of the relative error contribution estimates. (a), (c), and (d) are normalized with respect to the magnitude of the QoI at each iteration to produce the relative quantities.

Illustrated in Fig. 2(c) and Fig. 2(d), the proposed approach rapidly improves the mean and standard deviation of the cellwise relative error contribution estimates corresponding to the various tolerances used, with finer tolerances permitting greater enhancement of both quantities.

To examine the effect of the refinement on the exact and estimated relative error of the RCS, Fig. 3 illustrates the convergence of the computed RCS for the final discretizations produced with increasingly fine tolerances for $S1$. Note that as the estimated relative error is computed for the linearized QoI, the difference between the actual relative error and the estimated is due both to the inexactness of the error estimation *and* the linearization (as well as other deterministic sources

This article has been accepted for publication in IEEE Transactions on Antennas and Propagation. This article is the author's version which has not been fully edited and content may change prior to final publication. Citation information: DOI 10.1109/TAP.2022.3177424

8

of error, e.g., from numerical integration or the geometrical discretization itself). Each data point is associated with one of the four tolerances tested, with the finest tolerance requiring the most DoFs and likewise for the other tolerances. The estimated relative error is reported as part of the AMR process using (37), whereas the exact relative error is computed by comparing the approximate RCS to that computed through the Mie series solution. Despite that the refinement procedure of one tolerance is entirely independent of the other tolerances, the proposed approach yields consistent and rapid convergence with finer tolerances and, correspondingly, more DoFs. For the finest tolerance, the procedure results in a relative error of the RCS of under 1×10^{-3} for $S1$, a significant improvement (by several orders of magnitude) over the starting discretization. In terms of the estimated relative error, the AMR procedure provides very close agreement to the exact values for the four tolerances, with the coarsest tolerance slightly underestimating the relative error and the finest tolerance slightly overestimating the error.

Solving the same problem with a uniformly refined (i.e., non-adaptive) discretization, a relative error of just over 3×10^{-3} for the RCS is achieved by 7776 DoFs. In other words, for fewer DoFs, the adaptive refinement procedure produces a discretization that is more than three times as accurate for computing the RCS.
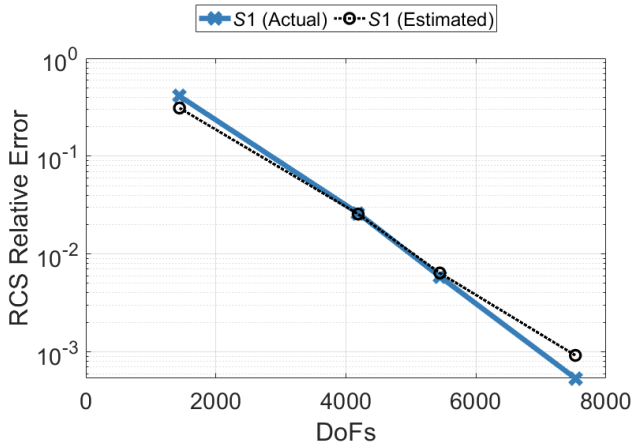
Fig. 3. Convergence of the actual and estimated relative errors for the monostatic RCS of the dielectric spherical scatterer $S1$.

As an illustration of the inherent mesh equilibration driven by the proposed method, Fig. 4 depicts the normalized cellwise error contributions for the starting discretization and the final discretization for the finest tolerance ($T_{\mathrm{rel}} = 1 \times 10^{-3}$) for the spherical scatterer $S1$. The starting discretization, shown in Fig. 4(a), exhibits extremely high error contribution concentration, indicating low efficiency and the overall low quality of the discretization. On the other hand, the discretization produced by the proposed AMR algorithm, Fig. 4(b), yields a significant reduction in error contribution concentration, with the estimates distributed about the discretization much more evenly, mirroring the results indicated by the significant improvement to the standard deviation of the error contributions in Fig. 2(d). Next, in Fig. 5(a) and Fig. 5(b), we examine
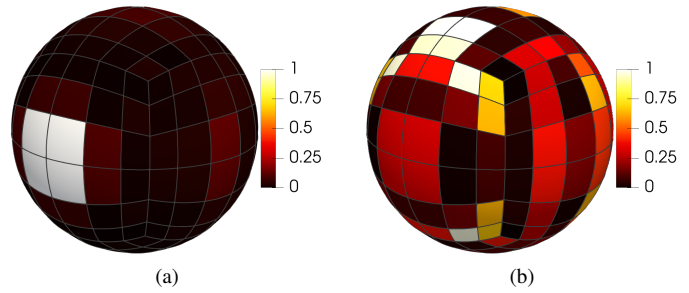

Fig. 4. Illustration of the error contribution estimate distributions for the dielectric scatter $S1$. (a) Normalized error contribution estimates for the starting discretization of $S1$. (b) Normalized error contribution estimates for the final discretization of $S1$ with $T_{\mathrm{rel}} = 1 \times 10^{-3}$. For the purposes of illustration, in (a) and (b) the error contribution estimates on each cell are normalized such that the smallest has a value of zero, and the largest a value of one.
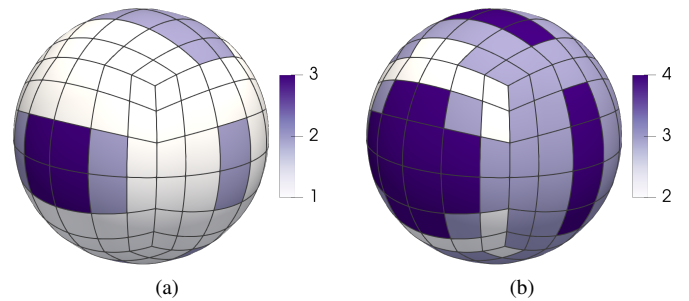

Fig. 5. Illustration of the expansion orders for the coarsest and finest tolerances of the dielectric spherical scatterer $S1$. (a) The final discretization for the coarsest tolerance T_{S1L1} of $S1$. (b) The final discretization for the finest tolerance T_{S1L4} of $S1$.

the final discretizations for $S1$ for the coarsest tolerance and finest tolerance, respectively. Both discretizations exhibit significant overlap in terms of the general refinement pattern. However, the finest tolerance demands a much greater degree of refinement globally.

Fig. 6 depicts the distribution of expansion orders for the final discretizations of each model and each tolerance. The coarse tolerances tested retain even first order basis functions, while, as expected, the finer tolerances require increasingly higher expansion orders. The finest tolerance of $S1$, for example, requires up to fourth-order basis functions. Overall, however, third-order basis functions are required most frequently. These results confirm those found in [19], which indicated that high accuracy computations typically require at least cubic or quartic polynomial bases.

Finally, Fig. 7 documents the total cost (in terms of the number of DoFs) of solving both the forward and adjoint problems as outlined in Section II and Section III for the four tolerances tested. While the adjoint solution dominates the cost of the coarsest tolerance, the forward solution comprises more than half cost for the finer tolerances, lessening the relative computational cost even with the rudimentary approach to discretizing the adjoint problem.

While the first example illustrates the capability of the approach to attain high accuracy for spherical scatterers, we now study its application to another canonical scattering target

This article has been accepted for publication in IEEE Transactions on Antennas and Propagation. This article the author's version which has not been fully edited and content may change prior to final publication. Citation information: DOI 10.1109/TAP.2022.3177424
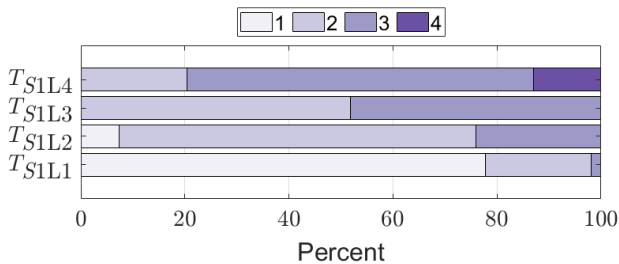
9

Fig. 6. The distribution of expansion orders for the spherical scatterer $S1$ for the four tolerances.
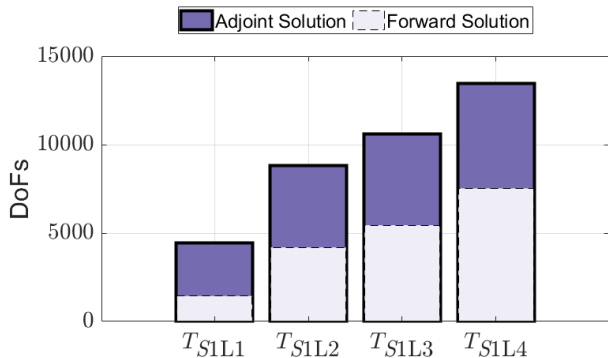
Fig. 7. The total cost (in terms of the number of DoFs) of solving both the forward and adjoint problems for the spherical scatterer $S1$ for the four tolerances.

in the form of the so-called NASA almond, introduced in [48]. In this case, the starting discretization—illustrated in Fig. 8—consists of 136 geometrically biquadratic cells with first order basis functions. Proceeding in an identical fashion to the spherical scatterer, we refer to this scatterer by $S2$. We test the scatterer for $\varepsilon_r = 4.5 - j0.05$, where the longest dimension of the almond is $3\lambda_0$ and we once again examine the monostatic RCS QoI through (25) with a planewave (polarized in the θ-direction as in Fig. 8) incident at the nose of the almond ($\theta = \pi/2$, $\phi = 0$).
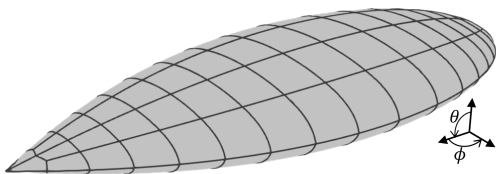
Fig. 8. The starting discretization for the NASA Almond scatterer $S2$ with 136 geometrically biquadratic elements and first order basis functions.

In contrast to the previous example, the reference RCS is now computed from a significantly uniformly refined mesh, both in h (twice as many elements) and p, and features 17408 DoFs. Geometrically, the relative error of the surface area of $S2$ compared to the reference model is 4.6×10^{-5}. However; in terms of the QoI, the RCS computed from the starting discretization yields a large percent error of 81% compared to this reference.

Once again, we define the relative local tolerance thresholds

to be

$$T_{S2Lj} = \alpha \frac{T_{\text{rel}j}}{136}, \qquad (40)$$

where j indexes the set of four previously chosen relative tolerances.

Illustrated in Fig. 9, the performance with the NASA almond is nearly identical to the example with the sphere. The proposed approach rapidly refines the discretization for all the tolerances. Of the four tolerances, the coarsest tolerance requires four iterations (making very small changes), whereas the remaining tolerances each require three iterations. Likewise, we see again that the first iteration contributes the most to the change in the discretization with the subsequent iterations offering much smaller adjustments. Lastly, as in spherical case, the mesh equilibration is greatly improved with enhancements to the mean and standard deviation of the relative error contribution estimates as seen in Fig. 9(c) and (d).

Next, in Fig. 10, we again see very similar performance in terms of the computation of the RCS. The estimated error in the RCS, which we again note is for the linearized quantity as discussed in Section II, closely matches that of the actual, with the second to last iteration slightly underestimating the error in the QoI, with an estimated relative error of 1.1×10^{-3} compared to the actual relative error of 1.9×10^{-3}. Moreover, for computing the RCS with non-adaptive, uniform refinements, a relative error of 2.3×10^{-4} requires 8704 DoFs, indicating that the proposed adaptivity, which achieves a relative error of 2.1×10^{-4} by 4448 DoFs, drives significantly improved error reduction efficiency. Even when compared to the coarser tolerances, uniform refinement requires 2176 DoFs to achieve a relative error of 2.9×10^{-2}.

In Fig. 11(a) and Fig. 11(b) we depict the distribution of the expansion orders for the final discretizations for the coarsest and finest tolerances, respectively, and Fig. 12 similarly depicts the distribution of the expansion orders for the final discretizations of the four tolerances tested for $S2$. Summarizing the total cost of solving the forward and adjoint problems for each of the tolerances, Fig. 13 reports the number of DoFs required for the solution of the two problems by the end of the refinement procedure, exhibiting a similar trend as seen for the spherical scatterer.

For the next two examples, we explore further the capability of the proposed approach to equilibrate error contributions within a discretization and across multiple problems, such as a range of scattering angles. Specifically, we first investigate a challenging example of monostatic scattering from a square PEC plate with side lengths of 8λ, as seen in Fig. 14. The discretization consists of 100 bilinear elements with first order basis functions. The monostatic scattering angle is swept from $\theta = 0$ to $\theta = \pi/2$ and the incident wave is polarized in the θ-direction. For this example, the RCS changes drastically, from very large at $\theta = 0$ to zero by $\theta = \pi/2$. We apply the same refinement process as before for each monostatic scattering angle separately and with a single desired relative tolerance of $T_{\text{rel}} = 1 \times 10^{-2}$ used with (38) and the linearized RCS QoI by means of (25) for all scattering angles. In practical applications, rather than treat each scattering direction separately,
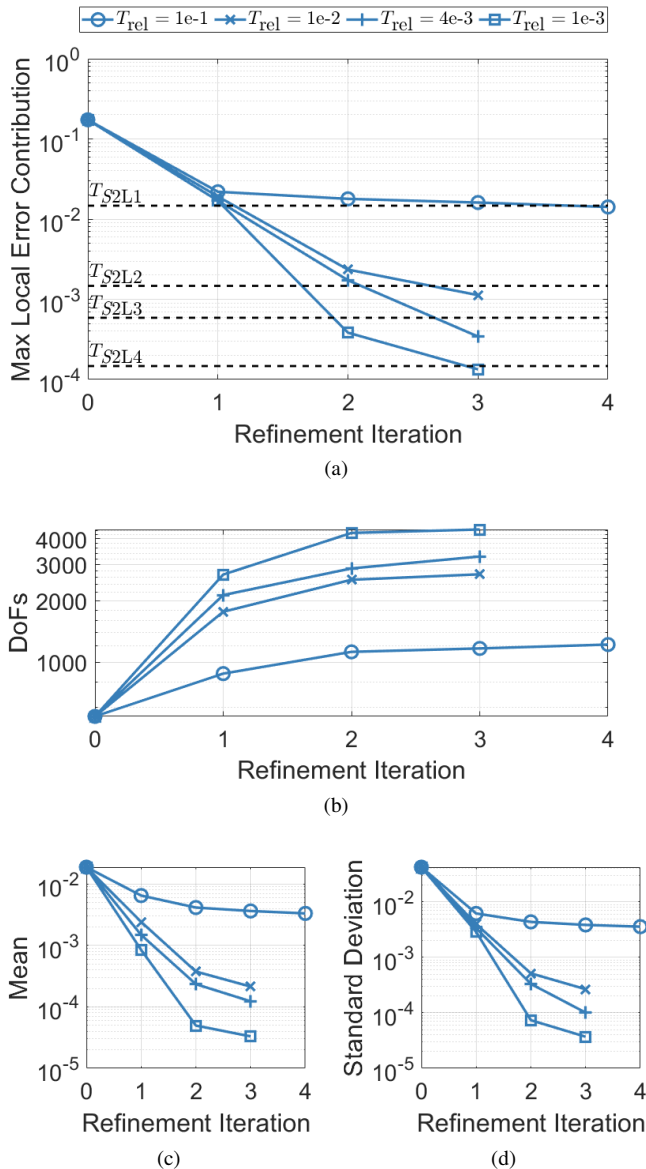
(a)

(b)

(c)

(d)

Fig. 9. Performance of the AMR algorithm for the NASA almond scatterer $S2$ for four tolerances. (a) Convergence of the relative maximum error contribution estimate versus the number of refinement iterations. (b) DoFs allocated by the AMR procedure at each iteration. (c) Mean of the relative error contribution estimates. (d) Standard deviation of the relative error contribution estimates. (a), (c), and (d) are normalized with respect to the magnitude of the QoI at each iteration to produce the relative quantities.

the QoIs could be clustered and combined, e.g., in the manner discussed in [15] for computing S-parameters. However, in order to specifically study the consistency and effectiveness of the refinement approach itself—in particular, the consistency of mesh equilibration—as opposed to that of the QoI clustering strategy, we consider the AMR procedure of each scattering angle independently.

The monostatic RCS computations from the uniformly refined reference discretization, the very coarse starting discretization, and the adaptively refined models are depicted in Fig. 15. The reference data was computed using a significantly refined discretization with 18240 DoFs. The starting discretization, with a median relative error of 1.0 for the
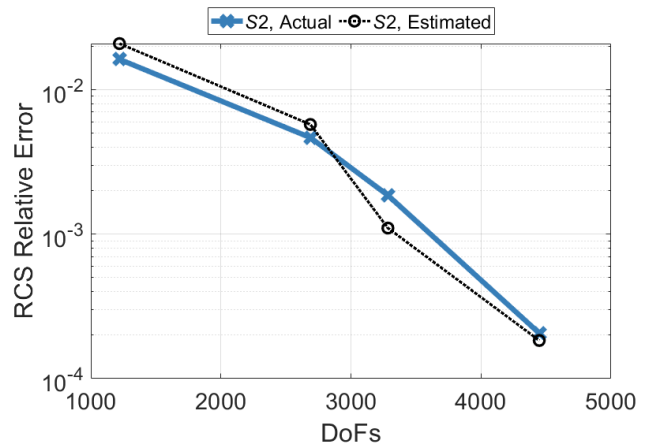
Fig. 10. Convergence of the actual and estimated relative errors for the monostatic RCS of the dielectric NASA almond scatterer $S2$.

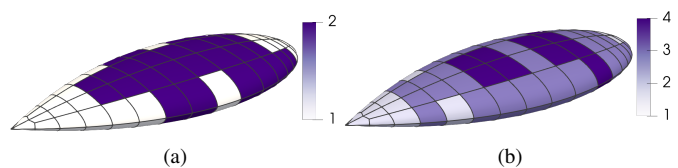
(a)   (b)

Fig. 11. Illustration of the expansion orders for the coarsest and finest tolerances of the dielectric NASA almond scatterer $S2$. (a) The final discretization for the coarsest tolerance T_{S2L1} of $S2$. (b) The final discretization for the finest tolerance T_{S2L4} of $S2$.
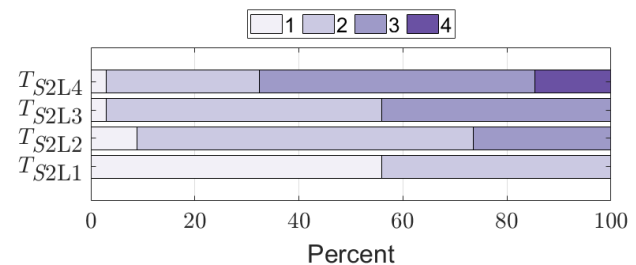

Fig. 12. The distribution of expansion orders for the NASA almond scatterer $S2$ for the four tolerances.
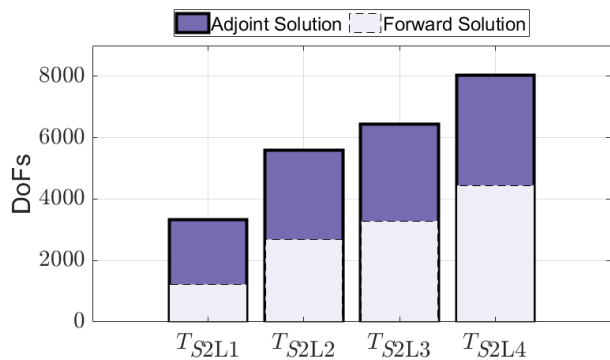

Fig. 13. The total cost (in terms of the number of DoFs) of solving both the forward and adjoint problems for the NASA almond scatterer $S2$ for the four tolerances.
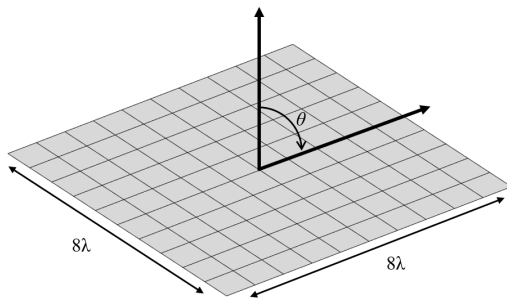
Fig. 14. The starting discretization for the square plate scatterer of dimension $8\lambda \times 8\lambda$ with 100 geometrically bilinear elements.
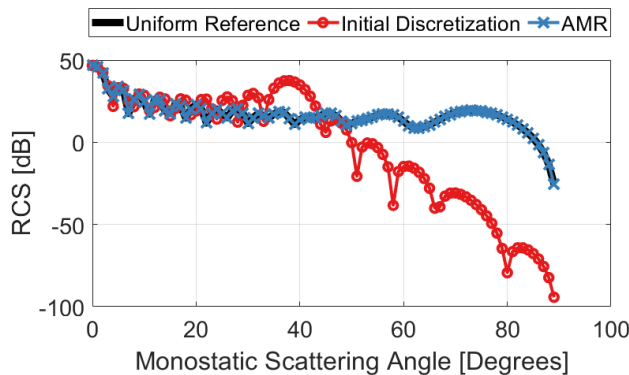

Fig. 15. The RCS (in dB) computed from the starting discretization and the adaptively refined discretizations compared to that of the uniformly refined reference for the square plate scatterer over a range of monostatic scattering angles.

RCS QoIs, yields extremely poor accuracy, particularly for the narrow scattering angles as the QoI approaches zero, while the AMR enables high accuracy across all scattering angles, with actual and estimated median relative errors of 1.5×10^{-2} and 9.8×10^{-3}, respectively, for the RCS QoIs, further indicating the ability of (38) to determine reasonable local tolerances without additional analysis, especially given the extreme coarseness of the discretization. Note that $\theta = 90$ is excluded, as the RCS is exactly 0.

Now, while the RCS differs substantially across the scattering angles, the equilibration properties of the proposed approach should yield discretizations of similar characteristics given the fixed desired relative error. To evaluate this capability, we measure the sample mean and dispersion of the relative cellwise error contribution estimates, both of which are sensitive to outliers in the data, to examine the consistency of the proposed approach over a wide-range of problems and QoIs in terms of mesh equilibration. The relative error contribution estimates are produced as in the previous examples by normalization according to the estimate of the monostatic RCS QoI, as the absolute tolerances, given the vastly different QoI magnitudes, differ substantially in value. Shown in Fig. 16, where the shaded bands contain two-thirds of the data and indicate the dispersion of the error contributions, the initial discretization features significant fluctuation in the mean and the dispersion of the relative error
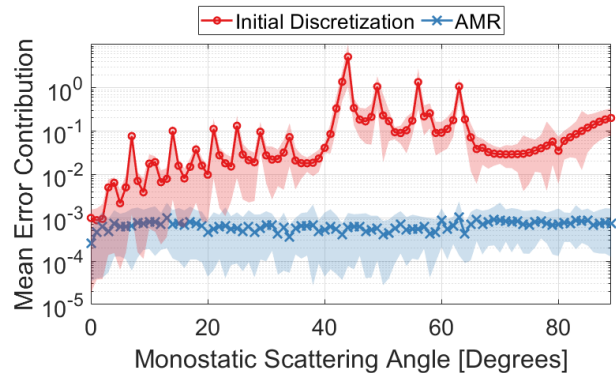

Fig. 16. Mean relative error contribution estimates (normalized according to the RCS at each scattering angle) with the dispersion illustrated by bands containing two-thirds of the data versus the scattering angle for the starting and final discretizations of the AMR procedure applied to the square plate scatterer.

contribution estimates as the scattering angle is swept from 0 to 90 degrees. However, after AMR, the discretizations yield near constant means and standard deviations for the relative error contribution estimates. The consistency of the AMR performance to successfully match the desired accuracy and, moreover, balance the discretization even when applied to a wide range of QoIs further indicates the efficiency of the proposed approach.

Lastly, as shown in Fig. 17, the modeling requirements to maintain the desired estimated relative error increase substantially until $\theta = 60$ degrees, at which point the required number of DoFs plateaus.
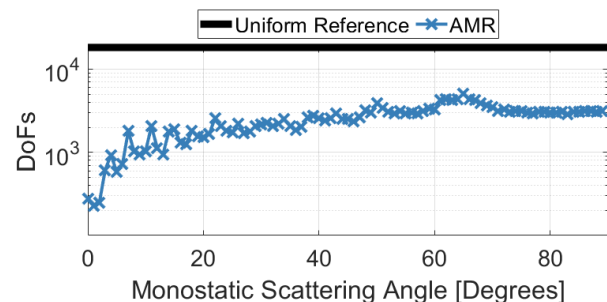

Fig. 17. The number of DoFs required by the AMR procedure compared to the uniformly refined reference for the square plate scatterer over a range of monostatic scattering angles.

For the final example, we revisit the same NASA almond scatterer from before with 136 geometrically biquadratic cells for the same relative permittivity and frequency. Here, we repeat the same analysis conducted for the square plate target, now with a fixed desired relative tolerance of $T_{\text{rel}} = 4 \times 10^{-3}$. Once again, we estimate the error in the monostatic RCS by means of the linearized quantity (25). The monostatic scattering angle is swept from the back of the almond ($\theta = -\pi/2$), over the top (with respect to the orientation in Fig. 8), to the nose of the almond ($\theta = \pi/2$).

In Fig. 18, we again examine the monostatic RCS for the reference model, the starting discretization, and the adaptively

refined discretization. The reference model is uniformly refined both in h and p, featuring 17408 DoFs. Except for $\theta = 0$, which is incidence on the top of the almond, the starting discretization is very poor, with extreme spikes in the computed RCS (for example, around $\theta = -20$). On the other hand, the adaptively refined models closely match the reference RCS values over the entire range of scattering angles. Specifically, for the adaptively refined models, the median relative error in the RCS is 1.9×10^{-3} and the median estimated relative error is 1.7×10^{-3}.
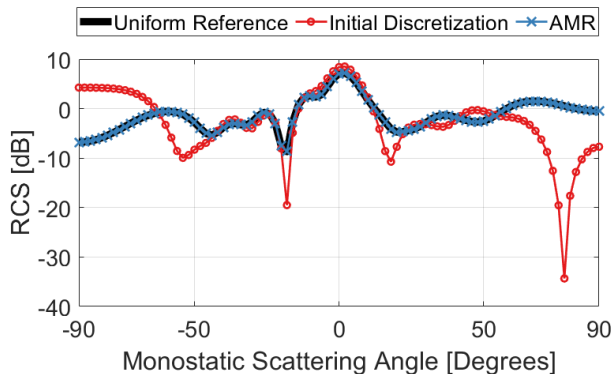

Fig. 18. The RCS (in dB) computed from the starting discretization and the adaptively refined discretizations compared to that of the uniformly refined reference for the dielectric NASA almond scatterer over a range of monostatic scattering angles.
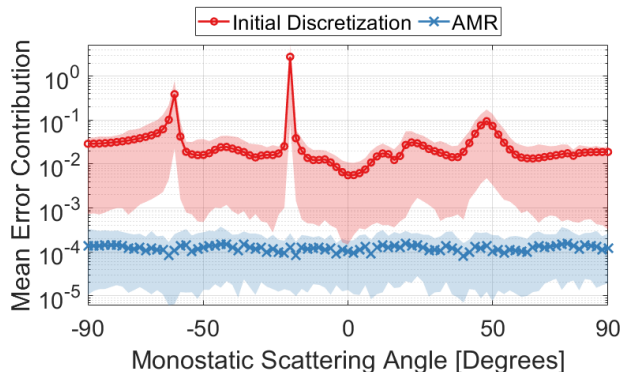

Fig. 19. Mean relative error contribution estimates (normalized according to the RCS at each scattering angle) with the dispersion illustrated by bands containing two-thirds of the data versus the scattering angle for the starting and final discretizations of the AMR procedure applied to the NASA almond scatterer.

Examining the mean and dispersion of the relative error contribution estimates as in Fig. 19, we see substantial variation in addition to large magnitudes. Conversely, the adaptively refined discretizations are nearly uniform throughout the entire range of scattering angles once again. For the large dip in the monostatic RCS for the starting discretization around $\theta = -20$, the estimated relative error approaches 100, and therefore the maximum degree of refinement, as noted in Section III, is limited to one; without this condition, a substantial degree of over-refinement would occur.
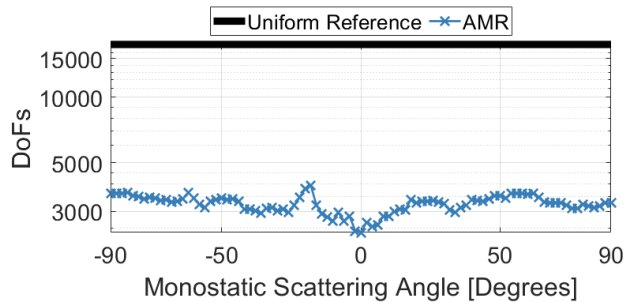

Fig. 20. The number of DoFs required by the AMR procedure compared to the uniformly refined reference for the NASA almond scatterer over a range of monostatic scattering angles.

Finally, in terms of the modeling requirements, Fig. 20 illustrates the number of DoFs allocated by the proposed refinement procedure for each scattering angle. The requirements are approximately symmetric with scattering from the nose and back of the almond posing the most challenge overall, whereas the large spike in error that occurs near the vicinity of $\theta = -20$ (seen in Figs. 18 and 19 for the initial discretization) requires a substantial boost in DoFs to alleviate to satisfaction of the QoI error tolerance.

As a result, for both the square plate and the NASA almond scatterer, the proposed method is effective at equilibrating the error contribution estimates, in addition to enhancing the quality of the discretizations for computing the RCS rapidly and providing accurate error estimates.

V. CONCLUSION

We have demonstrated an effective approach to mesh adaption and error control for general SIE problems in the EFIE and coupled EFIE-MFIE (PMCHWT) formulations. From a given tolerance, the proposed AMR procedure rapidly refines the discretization, producing accurate and efficient resource allocations even from extremely poor quality starting discretizations.

Along with studying the dual problems for the EFIE and the EFIE-MFIE (in the PMCHWT formulation), we provide a customizable and practical scattering QoI as well as a customizable linearized RCS QoI for directly tailoring discretizations through an explicit refinement algorithm. In concert with an effective methodology for producing high quality discretizations for the MoM-SIE, the provision of error estimates (as opposed to simply error indicators) greatly increases the confidence in the accuracy of simulation results.

Furthermore, by leveraging an *a priori* error behavior heuristic and goal-oriented *a posteriori* error estimation, our approach accelerates the refinement process, disconnecting the desired accuracy from the number of refinement iterations required and, as a result, permits practical refinement to high accuracy. Moreover, in producing simulations of customizable accuracy through adjustment of a single refinement tolerance, the approach significantly reduces the need for expert-user intervention.

Finally, the proposed approach encourages equilibrated error contribution estimates, indicating the high efficiency and

quality of the discretizations produced. Even when analyzing QoIs of varying magnitudes, the approach yields consistently balanced meshes.

A future work will study reducing the computational expense of generating the error estimates through cost-aware approximations of the adjoint solution.

ACKNOWLEDGMENT

REFERENCES

[1] M. Djordjevic and B. M. Notaros, "Double higher order method of moments for surface integral equation modeling of metallic and dielectric antennas and scatterers," *IEEE Transactions on Antennas and Propagation*, vol. 52, no. 8, pp. 2118–2129, 2004.

[2] B. M. Kolundzija and A. Djordjevic, *Electromagnetic Modeling of Composite Metallic and Dielectric Structures*. Norwood: Artech House, 2002.

[3] B. M. Kolundzija, "Electromagnetic modeling of composite metallic and dielectric structures," *IEEE Transactions on Microwave Theory and Techniques*, vol. 47, no. 7, pp. 1021–1032, 1999.

[4] L. F. Demkowicz, "Fully automatic hp-adaptivity for Maxwell's equations," *Computer Methods in Applied Mechanics and Engineering*, vol. 194, no. 2, pp. 605 – 624, 2005.

[5] D. Pardo and L. F. Demkowicz, "Integration of hp-adaptivity and a two-grid solver for elliptic problems," *Computer Methods in Applied Mechanics and Engineering*, vol. 195, no. 7, pp. 674–710, 2006.

[6] L. Demkowicz, *Computing with hp Finite Elements I. One- and Two-Dimensional Elliptic and Maxwell Problems*. Chapman & Hall/CRC Press, Taylor and Francis, 2007.

[7] M. M. Botha and D. B. Davidson, "An explicit a posteriori error indicator for electromagnetic, finite element-boundary integral analysis," *IEEE Transactions on Antennas and Propagation*, vol. 53, no. 11, pp. 3717–3725, Nov 2005.

[8] L. E. García-Castillo, D. Pardo, I. Gómez-Revuelto, and L. F. Demkowicz, "A two-dimensional self-adaptive hp finite element method for the characterization of waveguide discontinuities. Part I: Energy-norm based automatic hp-adaptivity," *Computer Methods in Applied Mechanics and Engineering*, vol. 196, no. 49, pp. 4823 – 4852, 2007.

[9] I. Gomez-Revuelto, L. E. Garcia-Castillo, S. Llorente-Romano, and D. Pardo, "A three-dimensional self-adaptive hp finite element method for the characterization of waveguide discontinuities," *Computer Methods in Applied Mechanics and Engineering*, vol. 249-252, pp. 62 – 74, 2012.

[10] S. M. Schnepp, "Error-driven dynamical hp-meshes with the discontinuous galerkin method for three-dimensional wave propagation problems," *Journal of Computational and Applied Mathematics*, vol. 270, pp. 353 – 368, 2014.

[11] P. Monk and E. Süli, "The adaptive computation of far-field patterns by a posteriori error estimation of linear functionals," *SIAM Journal on Numerical Analysis*, vol. 36, no. 1, pp. 251–274, 1998.

[12] P. Monk, "A posteriori error indicators for Maxwell's equations," *Journal of Computational and Applied Mathematics*, vol. 100, no. 2, pp. 173 – 190, 1998.

[13] L. E. G. Castillo, D. Pardo, and L. F. Demkowicz, "Fully automatic hp adaptivity for electromagnetics, application to the analysis of H-plane and E-plane rectangular waveguide discontinuities," in *2007 IEEE/MTT-S International Microwave Symposium*, 2007, pp. 285–288.

[14] L. E. Garcia-Castillo, D. Pardo, and L. F. Demkowicz, "Energy-norm-based and goal-oriented automatic *hp* adaptivity for electromagnetics: Application to waveguide discontinuities," *IEEE Transactions on Microwave Theory and Techniques*, vol. 56, no. 12, pp. 3039–3049, 2008.

[15] D. Pardo, L. E. García-Castillo, L. F. Demkowicz, and C. Torres-Verdín, "A two-dimensional self-adaptive hp finite element method for the characterization of waveguide discontinuities. Part II: Goal-oriented hp-adaptivity," *Computer Methods in Applied Mechanics and Engineering*, vol. 196, no. 49, pp. 4811–4822, 2007.

[16] D. Pardo, L. Demkowicz, C. Torres-Verdín, and M. Paszynski, "A self-adaptive goal-oriented hp-finite element method with electromagnetic applications. Part II: Electrodynamics," *Computer Methods in Applied Mechanics and Engineering*, vol. 196, no. 37, pp. 3585 – 3597, 2007.

[17] A. Zdunek and W. Rachowicz, "A goal-oriented hp-adaptive finite element approach to radar scattering problems," *Computer Methods in Applied Mechanics and Engineering*, vol. 194, no. 2, pp. 657 – 674, 2005.

[18] C. Key, A. P. Smull, D. Estep, T. Butler, and B. M. Notaroš, "A posteriori error estimation and adaptive discretization refinement using adjoint methods in CEM: A study with a 1-d higher order fem scattering example," *IEEE Transactions on Antennas and Propagation*, vol. 68, no. 5, pp. 3791–3806, 2020.

[19] J. J. Harmon, C. Key, D. Estep, T. Butler, and B. M. Notaroš, "Adjoint-based accelerated adaptive refinement in frequency domain 3-D finite element method scattering problems," *IEEE Transactions on Antennas and Propagation*, vol. 69, no. 2, pp. 940–949, 2021.

[20] W. Bangerth and R. Rannacher, *Adaptive Finite Element Methods for Differential Equations*. Birkhauser Basel, 2003.

[21] G. I. Marchuk, *Adjoint Equations and Analysis of Complex Systems*. Netherlands: Kluwer Academic Publishers, 1995.

[22] D. Estep, M. Holst, and D. Mikulencak, "Accounting for stability: A posteriori error estimates based on residuals and variational analysis," *Communications in Numerical Methods in Engineering*, vol. 18, pp. 15 – 30, 11 2001.

[23] M. H. Bakr and N. K. Nikolova, "An adjoint variable method for time domain TLM with fixed structured grids," in *IEEE MTT-S International Microwave Symposium Digest, 2003*, vol. 2, June 2003, pp. 1121–1124 vol.2.

[24] N. K. Nikolova, H. W. Tam, and M. H. Bakr, "Sensitivity analysis with the FDTD method on structured grids," *IEEE Transactions on Microwave Theory and Techniques*, vol. 52, no. 4, pp. 1207–1216, April 2004.

[25] S. M. Ali, N. K. Nikolova, and M. H. Bakr, "Central adjoint variable method for sensitivity analysis with structured grid electromagnetic solvers," *IEEE Transactions on Magnetics*, vol. 40, no. 4, pp. 1969–1971, July 2004.

[26] Y. Zhang, M. H. Negm, and M. H. Bakr, "An adjoint variable method for wideband second-order sensitivity analysis through FDTD," *IEEE Transactions on Antennas and Propagation*, vol. 64, no. 2, pp. 675–686, 2016.

[27] M. H. Bakr, *Nonlinear Optimization in Electrical Engineering with Applications in MATLAB*. IET, September 2013.

[28] S. Koziel and A. Bekasiewicz, "Fast EM-driven size reduction of antenna structures by means of adjoint sensitivities and trust regions," *IEEE Antennas and Wireless Propagation Letters*, vol. 14, pp. 1681–1684, 2015.

[29] E. Ubeda and J. M. Rius, "Novel monopolar MFIE MoM-discretization for the scattering analysis of small objects," *IEEE Transactions on Antennas and Propagation*, vol. 54, no. 1, pp. 50–57, 2006.

[30] E. Ubeda, J. M. Rius, and A. Heldring, "Nonconforming discretization of the electric-field integral equation for closed perfectly conducting objects," *IEEE Transactions on Antennas and Propagation*, vol. 62, no. 8, pp. 4171–4186, 2014.

[31] M. M. Bibby and A. F. Peterson, "On the use of overdetermined systems in the adaptive numerical solution of integral equations," *IEEE Transactions on Antennas and Propagation*, vol. 53, no. 7, pp. 2267–2273, 2005.

[32] U. Saeed and A. F. Peterson, "Explicit local error estimators for electromagnetic integral equations," *IEEE Transactions on Antennas and Propagation*, vol. 63, no. 3, pp. 1159–1163, 2015.

[33] S. K. Kim and A. F. Peterson, "Evaluation of local error estimators for the RWG-based EFIE," *IEEE Transactions on Antennas and Propagation*, vol. 66, no. 2, pp. 819–826, 2018.

[34] ——, "Adaptive h-refinement for the RWG-based EFIE," *IEEE Journal on Multiscale and Multiphysics Computational Techniques*, vol. 3, pp. 58–65, 2018.

[35] S. K. Kim, "Error estimation and adaptive refinement technique in the method of moments," Ph.D. dissertation, Georgia Institute of Technology, 2017.

[36] J. A. Tobon Vasquez, Z. Peng, J. F. Lee, G. Vecchi, and F. Vipiana, "Automatic localized nonconformal mesh refinement for surface integral

This article has been accepted for publication in IEEE Transactions on Antennas and Propagation. This is the author's version which has not been fully edited and content may change prior to final publication. Citation information: DOI 10.1109/TAP.2022.3177424

14

equations," *IEEE Transactions on Antennas and Propagation*, vol. 68, no. 2, pp. 967–975, 2020.

[37] P. I. Cilliers and M. M. Botha, "Goal-oriented error estimation for the method of moments to compute antenna impedance," *IEEE Antennas and Wireless Propagation Letters*, vol. 19, no. 6, pp. 997–1001, 2020.

[38] A. Poggio and E. Miller, "Integral equation solutions of three-dimensional scattering problems," in *Computer Techniques for Electromagnetics*, ser. International Series of Monographs in Electrical Engineering. Pergamon, 1973, pp. 159–264.

[39] Y. Chang and R. Harrington, "A surface formulation for characteristic modes of material bodies," *IEEE Transactions on Antennas and Propagation*, vol. 25, no. 6, pp. 789–795, 1977.

[40] T. Wu and L. L. Tsai, "Scattering from arbitrarily-shaped lossy dielectric bodies of revolution," *Radio Science*, vol. 12, no. 5, pp. 709–718, 1977.

[41] A. Peterson, D. Wilton, and R. Jorgenson, "Variational nature of galerkin and non-galerkin moment method solutions," *IEEE Transactions on Antennas and Propagation*, vol. 44, no. 4, pp. 500–503, 1996.

[42] K. Chen, "Error equidistribution and mesh adaptation," *SIAM Journal on Scientific Computing*, vol. 15, no. 4, pp. 798–818, 1994.

[43] A. Bespalov and N. Heuer, "Natural hp-BEM for the electric field integral equation with singular solutions," 2010.

[44] P. Houston, B. Senior, and E. Süli, "Sobolev regularity estimation for hp-adaptive finite element methods," *Numerical Mathematics and Advanced Applications*, pp. 619–644, 2003.

[45] I. Babuška and M. Suri, "The p and h-p versions of the finite element method, basic principles and properties," *SIAM Review*, vol. 36, no. 4, pp. 578–632, 1994.

[46] B. Guo and I. Babuška, "The h-p version of the finite element method," *Computational Mechanics*, vol. 1, no. 1, pp. 21–41, 1986.

[47] W. Dörfler, "A convergent adaptive algorithm for Poisson's equation," *SIAM Journal on Numerical Analysis*, vol. 33, no. 3, pp. 1106–1124, 1996.

[48] A. Woo, H. Wang, M. Schuh, and M. Sanders, "EM programmer's notebook-benchmark radar targets for the validation of computational electromagnetics programs," *IEEE Antennas and Propagation Magazine*, vol. 35, no. 1, pp. 84–89, 1993.

Branislav M. Notaroš (M'00–SM'03–F'16) received the Dipl.Ing. (B.S.), M.S., and Ph.D. degrees in electrical engineering from the University of Belgrade, Belgrade, Yugoslavia, in 1988, 1992, and 1995, respectively.

From 1996 to 1999, he was Assistant Professor in the School of Electrical Engineering at the University of Belgrade. He was Assistant and Associate Professor from 1999 to 2006 in the Department of Electrical and Computer Engineering at the University of Massachusetts Dartmouth. He is currently Professor of Electrical and Computer Engineering, University Distinguished Teaching Scholar, and Director of Electromagnetics Laboratory at Colorado State University.

Dr. Notaroš serves as General Chair of the 2022 IEEE International Symposium on Antennas and Propagation and USNC-URSI Radio Science Meeting and is Track Editor for the IEEE Transactions on Antennas and Propagation. He serves as President of Applied Computational Electromagnetics Society (ACES), as Chair of USNC-URSI Commission B, and as Meetings Committee Chair for the IEEE Antennas and Propagation Society. He was the recipient of the 2005 IEEE MTT-S Microwave Prize, 1999 IEE Marconi Premium, 2019 ACES Technical Achievement Award, 2015 ASEE ECE Distinguished Educator Award, 2015 IEEE Undergraduate Teaching Award, and many other research and teaching international and national awards.
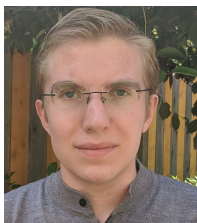
Jake J. Harmon (S'19) was born in Fort Collins, CO in 1996. He received the B.S. degree (*summa cum laude*) in Electrical Engineering from Colorado State University, Fort Collins, CO, USA, in 2019, where he is currently pursuing the Ph.D. degree in Electrical Engineering.

His current research interests include adaptive numerical methods, uncertainty quantification, computational geometry, and higher order modeling in the finite element method and surface integral equation method of moments.